

Design of Multiband Slot Antenna for GPS/Wimax /WLAN Systems.

Sayali S. Pawar, Jagadish B. Jadhav

Department of Electronics and Telecommunication Engg, R.C Patel Institute of Technology, Shirpur, Dhule.
Department of Electronics and Telecommunication Engg, R.C Patel Institute of Technology, Shirpur, Dhule

Corresponding Author: Sayali S. Pawar

ABSTRACT— A design approach of antenna for Global positioning system (GPS), worldwide interoperability for microwave access (Wimax), and wireless area network (WLAN) systems is presented. The antenna was studied by means of simulations as well practical measurements. The tri-band characteristics of antenna are due to rectangular slot with T-shaped feed patch, an inverted T-shaped stub and two E-shaped stubs on the radiating structure. The Proposed antenna achieves return loss (greater than -10db), radiation patterns, peak gain and efficiency gain at all three operating bands. The antenna is simulated using IE3d software. Quantified results shows that antenna can be designed to cover frequency bands for all three wireless systems. The simulated and quantified results of antenna are in good agreement.

Keywords- Global positioning system (GPS), multiband antenna, slot antenna, wireless area network (WLAN), worldwide interoperability for microwave access (WiMax).

Date Of Submission: 26-04-2019

Date Of Acceptance: 06-05-2019

I. INTRODUCTION

With the developments of many different wireless communications standards, it is desirable to integrate as many standards such as the Global positioning situating system (GPS), worldwide interoperability for microwave access (WiMAX), and wireless area network (WLAN) standards as possible into a single wireless device. For this reason, different multiband antennas have been studied, e.g., the dual-band monopole antenna for the WiMAX systems in [1], the multiband planar inverted-F antenna (PIFA) for the wireless wide area network (WWAN) system in [2], the multiband patch antenna having varied polarization states in [3], and the dual-band loop antenna for the 2.4/5.2/5.8 GHz bands in [4]. Slot antenna, with the advantages of compact size, wide bandwidth, and facile integration with other contrivances is a good candidate for the design of multiband antennas. In the past years, different designs of multiband slot antennas have been proposed [5]–[13]. The dual-band characteristics of the slot antennas in [5], [6], and [7], [8] were generated by etching several narrow slots on the ground planes or several stubs on the immensely colossal slots, respectively. The tri-band antennas in [9], [10] and [11], [12] were achieved utilizing three folded slots etched on the ground planes or several stubs on the slots, respectively. Among these tri-band slot antennas, the one in [10] had the most diminutive radiating portion of $0.46\lambda_g \times 0.2\lambda_g$ (where λ_g is the guide wavelength), and the one in [12] achieved the most minuscule total size of $0.44\lambda_g \times 0.38\lambda_g$. A four-

band slot antenna was proposed in [13] utilizing several stubs on the ultra-wideband slot radiator. The antenna had a very compact size of only $0.24\lambda_g \times 0.21\lambda_g$, but a peak gain of only -6 to -4 dB in the frequency band of 1.5–3 GHz, which is too minute for practical uses. In this paper, we present the design of a four-band slot antenna for the GPS/WiMAX/WLAN systems. The antenna consists of a rectangular slot, a T-shaped feed patch, an inverted T-shaped stub, and two E-shaped stubs to engender four frequency bands at about 1.575, 2.45, 3.5, and 5.4 GHz for the GPS, IEEE 802.11b&g, WiMAX, and IEEE 802.11a systems, respectively. It should be noted that since each frequency band is engendered utilizing only one antenna element, the proposed antenna cannot support the optional MIMO feature designated in the **WiMAX standard**. Unlike antenna tri-band designs [9]–[12], in which each frequency band was engendered utilizing A slot, in the proposed four-band antenna, we utilize the **harmonics of the T-shaped feed patch** to engender two frequency bands. Then utilizing a double-folded **stub in the T-shaped feed patch**, the two harmonic resonant frequency can be tuned independently. With this method, the slot antenna can have four operating bands and a size more minute than those of the tri-band antennas studied in [9]–[12]. The radiating portion of the proposed antenna has a compact size of only $0.43\lambda_g \times 0.17\lambda_g$ (which is 25% more minute than the tri-band antenna in [10]) and a total size of $0.43\lambda_g \times 0.34\lambda_g$ (which is 14% more minuscule than the tri-band antenna in [12]). The gains

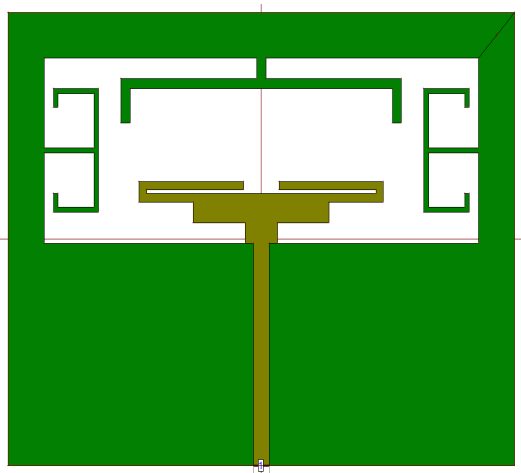


Fig. 1. Geometry of proposed antenna

of the antenna in the four frequency bands are much higher gains than those of the four-band antenna in [13]. The proposed multiband antenna is studied and designed utilizing the IE3D Software. The methodology used to design the antenna for other frequency bands is additionally proposed. For verification of simulation results, the antenna is fabricated and quantified. The results on reflection coefficient S_{11} , radiation pattern, realized peak gain, and efficiency are presented. The frequency bands 2.4–2.545 GHz for the IEEE 802.11b&g WLAN systems, 3.27–3.97 GHz for the WiMAX system, and 5.17–5.93 GHz for the IEEE 802.11a WLAN system. The effects of the feeding cable utilized in quantification and of the cover are additionally investigated.

II. ANTENNA DESIGN.

The proposed multiband slot antenna is shown in Fig. 2, which consist of a rectangular slot with a size $L1 \times W1 = 48 \times 18 \text{ mm}^2$ on one side of the substrate. The rectangular slot is loaded with an inverted T-shaped stub at the upper edge of the rectangular slot and two E-shaped stubs on the left-hand (LH) and right-hand (RH) sides of the slot. The inverted T-shaped stub has the horizontal strip folded on both sides to achieve a compact size. A T-shaped feed patch with micro strip victualed on the other side of the substrate is utilized to victual the rectangular slot. The element line has a width of $Wf = 1.76 \text{ mm}$ to achieve an impedance of 50Ω . The upper side of the T-shaped patch is elongated on both sides and then double-folded to achieve a compact size.

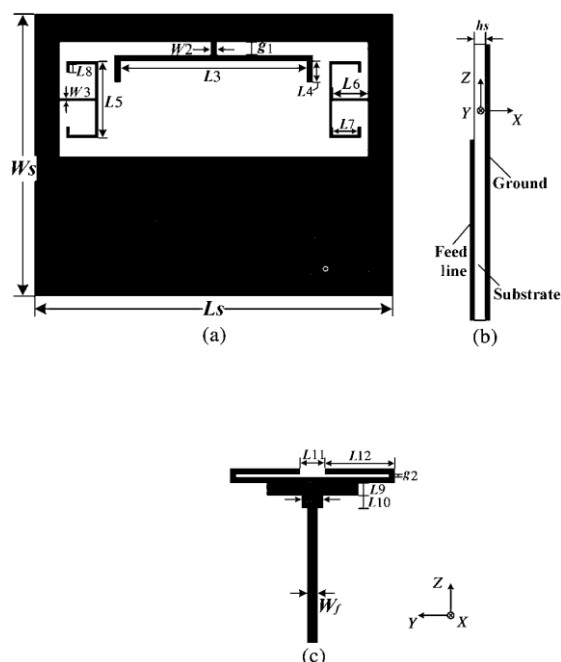


Fig. 2. Geometry of antenna: (a) top view; (b) side view; and (c) bottom view (dark gray—metal in front and light gray—metal in bottom).

A step is utilized in the lower side of the T-shaped aliment patch on both the LH and the RH sides for better impedance matching. The antenna can engender four frequency bands at about 1.575, 2.45, 3.5, and 5.4 GHz, denoted here as bands 1, 2, 3, and 4, respectively, for different wire- less standards. The rectangular slot and the inverted T-shaped stub together engender band 1 at about 1.575 GHz for the GPS system. The two E-shaped stubs operating as monopole radiators engender band 2 at about 2.45 GHz for the IEEE 802.11b&g WLAN systems. The T-shaped aliment patch and inverted T-shaped stub engender band 3 at about 3.5 GHz for the WiMAX system. The T-shaped aliment patch in the higher mode engenders band 4 at about 5.4 GHz for the IEEE 802.11a WLAN system. The antenna is studied and designed on a substrate with a relative permittivity of $\epsilon_r = 3.5$, a thickness of

Table 1. DIMENSIONS OF THE PROPOSED ANTENNA (MM)

L1	L2	L3	L4	L5	L6	L7	L8	L9
48	21.6	29	3.3	12	5.5	4	1.3	2
L10	L11	L12	g1	g2	W1	W2	W3	W4
2	4	11.5	2	0.4	18	1	0.5	3.6
W5	Wf	Ws	hs	Ls				
15	1.76	44	0.8	56				

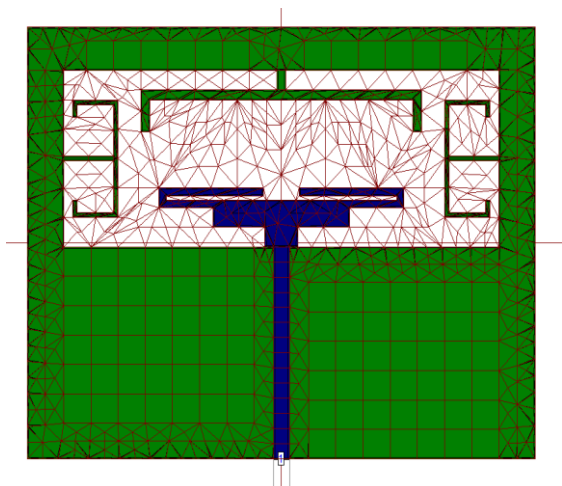


Fig. 3. Geometry of antenna Current Distribution.

0.8 mm, and a loss tangent of 0.004. The final dimensions of the multiband antenna are given in Table I, which is utilized to fabricate the antenna shown in Fig. 2 for quantification. In the antenna layout shown in Fig. 1, the victual line is placed symmetrically on the sizably voluminous ground plane, which could be occluding the way for other electronic components placed on the printed circuit board (PCB). However, the aliment line could withal be designed to have a 90° bent or be placed asymmetrically on the ground plane to give more space for other components. Since most other designs have the victual lines placed symmetrically on the ground plane, for facile comparison made by others, we withal place the aliment line symmetrically on the ground plane in our design.

III. DESIGN PARAMETERS OF ANTENNA.

The length and width of the basic patch according to the

Desired frequency are as follows.

Width of the patch (W):

$$W = \frac{c}{2f_0} \sqrt{\frac{2}{\epsilon_r + 1}} \quad (1)$$

Length (L) is given by,

$$L = \frac{\lambda_0}{2\sqrt{\epsilon_{\text{reff}}}} - 2\Delta L \quad (2)$$

Where,

$$\Delta L = 0.412h \frac{(\epsilon_{\text{eff}} + 0.3)\left(\frac{W}{h} + 0.262\right)}{(\epsilon_{\text{eff}} - 0.258)\left(\frac{W}{h} + 0.813\right)} \quad (3)$$

$$\epsilon_{\text{reff}} = \frac{\epsilon_r + 1}{2} + \frac{\epsilon_r - 1}{2} \left[1 + \frac{12h}{W} \right]^{-1/2} \quad (4)$$

Studies Of Antenna

To study the effects of different radiating elements on the frequency bands of the proposed multiband antenna, computer simulation on S11 is carried out in four conditions: 1) only the T -shaped victual patch; 2) only the T -shaped aliment patch and the inverted T -shaped stub; 3) only the T -shaped victual patch and the two E-shaped stubs; and 4) the consummated design (proposed antenna). Results with captioned conditions are shown in Fig. 3. It can be optically discerned that, in condition 1 when only the T -shaped aliment patch is utilized in the slot, the antenna engenders three frequency bands, bands 1, 3, and 4, at about 1.8, 3.5, and 5.2 GHz, respectively. (Current distribution shown later betokens that band 1 at 1.8 GHz is engendered mainly by the rectangular slot, and bands 3 and 4 at 3.5 and 5.2 GHz, respectively, are mainly engendered by the T -shaped victual patch in different modes.) In condition 2, when the inverted T -shaped stub is integrated, Fig. 3 shows that band 1 is moved scarcely down from 1.8 to 1.575 GHz, yet bands 3 and 4 remaining about equipollent. If the two E-shaped stubs are utilized, in lieu of the inverted T -shaped stub, as in condition 3, Fig. 3 shows that the antenna has four frequency bands, bands 1, 2, 3, and 4, at about 1.8, 3.5, 2.5, and 5.2 GHz, respectively thus, one more frequency band (with quite an impotent resonance) is engendered at about 2.5 GHz. Moreover, the bandwidth of band 4 at about 5.2 GHz is widened. However, in condition 4, when all the elements are utilized, Fig. 3 shows that the proposed multi- band antenna has four frequency bands (with S11 < -10 dB), i.e., 1.522–1.588 GHz for the GPS system, 2.368–2.56 GHz for the IEEE 802.11b&g WLAN systems, 3.19–3.832 GHz for the WiMAX system, and 4.96–5.94 GHz for the IEEE 802.11a WLAN system. Note that the WiMAX application has been assigned different frequency bands such as at 2.3, 2.5, 3.5, 3.7 and 5.8 GHz. The 2.5-GHz and 5.8-GHz WiMAX bands overlap with the IEEE 802.11b&g and IEEE 802.11a WLAN bands, respectively, which are supplementally covered by the proposed antenna. Thus, the proposed antenna can cover proximately all these WiMAX bands. Albeit the GPS system employs circularly polarized (CP) signal with a frequency band from 1570 to 1590 MHz, most commercial wireless contrivances employ linearly polarized antennas to receive the GPS signal. This will lead to a 3-dB power loss, but it is commonly acceptable by wireless contrivance designers. Thus, our linearly polarized antenna with the lowest band from 1.575 to 1.665 GHz can be utilized for the GPS system.

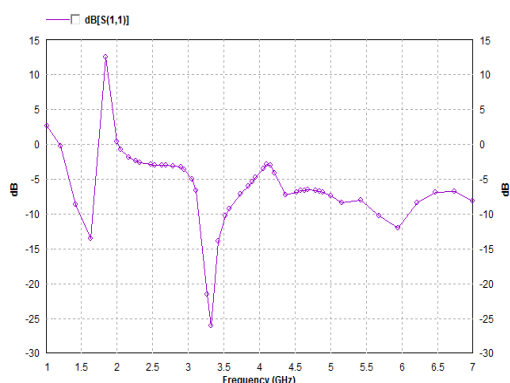


Fig. 4. Simulated S11 using different radiating elements of antenna.

The geometry of the antenna shown in Fig. 1(a) has many parameters such as L1, L3-L10, W1, W5, and g1, which would affect the frequency bands. In order to utilize the design in different applications, we require to find the parameters and a method to facilitate set the frequencies of these frequency bands. Thus, computer simulation has been used to study the effects of different parameters on the four frequency bands. In the study, we kept the antenna size (i.e., the slot area $W \times L1$) unchanged. Results have showed that we can set the frequency bands in the order of bands 3, 4, 1, and 2 utilizing the following parameters.

- Band 1: Using g1 (the gap between the inverted T-shaped stub and the upper edge of the slot).
- Band 2: Using L6 (the height of the E-shaped stub)
- Band 3: Using L3 (the length of the inverted T-shaped stub) and W5 (width of the T-shaped feed patch).
- Band 4: Using L12 (the length of the double-folded stub in the T-shaped feed patch).

The results of parametric study on these parameters are shown in Fig. 4. With L3 incremented from 23 mm to 26 and 29 mm, Fig. 4(a) shows that the low-cutoff frequency (for $S_{11} < -10$ dB) of band 3 shifts from 3.43 GHz to 3.28 and 3.19 GHz, respectively. (Note that L3 additionally scarcely affects band 2, but it can be adjusted back utilizing L6 as shown later.) With W5 incremented from 8 mm to 11 and 15 mm, Fig. 4(b) shows that the high-cutoff frequency of band 3 shifts from 3.63 GHz to 3.73 and 3.83 GHz, respectively. Thus, L3 and W5 can be acclimated to set the frequency for band 3. With L12 incremented from 10.2 to 11.5 and 12.8 mm, Fig. 4(c) shows that band 4 shifts from 5.69 GHz to 5.30 and 5.02 GHz, respectively, with other bands remaining about identically tantamount. So, L12 can be habituated to set band 4. With g1 incremented from 1 mm to 2 and 3 mm, Fig. 4(d) shows that band 1 shifts from 1.62 GHz to 1.55 and 1.49 GHz, respectively.

Albeit g1 additionally scarcely affects band 2, this can be adjusted back utilizing L6. Fig. 4(e) shows that as L6 increases from 5 mm to 5.5 and 6.0 mm, band 2 shifts from 2.47 GHz to 2.41 and 2.34 GHz, respectively, yet the other frequency bands remaining about equipollent. Thus, L6 can be acclimated to set band 2. The ground-plane size of the antenna has significant effects on the performance, so a parametric study is carried out on L2, which determines the ground-plane size. The simulated S11 in Fig. 4(f) shows that, with L2 incremented from 16 mm to 21.6 and 24 mm, band 1 shifts from 1.575 GHz to 1.552 and 1.54 GHz, band 2 shifts from 2.395 GHz to 2.41 and 2.425 GHz, band 3 shifts from 3.445 GHz to 3.406 and 3.375 GHz, and band 4 shifts from 5.255 GHz to 5.302 and 5.315 GHz. It can be visually perceived that the transmutations in frequency are relatively diminutive as L2 increases from 16 mm to 21.6 and 24 mm, but the matching in all four bands is significantly amended. Thus the ground-plane size avails achieve better matching. The operation of the antenna is further studied utilizing current distribution at the resonant frequencies as shown in Fig. 5. At 1.575 GHz for band 1, Fig. 5(a) shows that the surface current mainly distributes at the edges of the rectangular slot, with some on the inverted T-shaped stub. The resonant frequency f1 can roughly be resolute by the slot dimension, i.e.

$$f_1 = \frac{c}{2(L1 + W1) \cdot \sqrt{\epsilon}} = 1.43 \text{ GHz} \quad (1)$$

where ϵ is the efficacious dielectric constant given by $\epsilon \approx (\epsilon_r + 1)/2 = 2.25$ with ϵ_r being the relative permittivity of the substrate, c is the haste of light in free space, and L1 and W1 are the length and width, respectively, of the rectangular slot. Fig. 5(a) betokens that the inverted T-shaped stub increases the current path along the slot edges and hence lowers down the resonant frequency as denoted in Fig. 3. Moreover, the parameter g1 affects the length of the current path and consequently can be habituated to adjust band 1 as shown in Fig. 4(d). At 2.45 GHz for band 2, Fig. 5(b) shows that the current mainly concentrates on the two E-shaped stubs, which accommodate as monopole radiators with resonant frequency approximately given by [11], [12]

$$f_2 = \frac{c}{4(L6 + L5/2 + L7 + L8) \cdot \sqrt{\epsilon}} = 2.98 \text{ GHz} \quad (2)$$

Where L6, L5, and L7 are as denoted in Fig. 1(a); thus, L6 can be acclimated to adjust the frequency for band 2 as shown in Fig. 4(e). Fig. 5(b) designates that some currents are coupled to the inverted T-shaped stub, which lowers down the resonant frequency from 2.5 to 2.45 GHz as shown in Fig. 3. At 3.5 GHz for band 3, Fig. 5(c) shows that currents flow along the double-folded extended stubs of the T-shaped feed patch and also on the inverted T-shaped stub, thus both elements deter- mine the

frequency. At 5.2 GHz for band 4, Fig. 5(d) shows that the current mainly flows on the T-shaped feed patch which is similar to that of Fig. 4(c) at 3.5 GHz but with a shorter wavelength, indicating higher mode operation. With these results, we propose to set the frequency bands of the multiband antenna using the following steps:

- 1) Use the dimensions in Table I to start with
- 2) Use L3 and W5 to roughly set band 3
- 3) Use L12 to set band 4
- 4) Use g1 to roughly set band 1
- 5) Use L6 to set band 2
- 6) Use all these parameters to fine-tune the design.

Simulation has shown that, with the use of the above steps, the center frequencies of the four frequency bands have the tuning ranges listed in Table II.

IV. SIMULATION AND MEASUREMENT RESULTS.

The proposed multiband antenna has been studied utilizing computer simulation. The prototyped antenna of Fig. 2 has withal been quantified utilizing the antenna quantification equipment, Satimo StarLab System [14]. The simulated and quantified S11 are shown in Fig. 4. It can be visually perceived that the antenna has four frequency bands. The quantified frequency bands (for S11 < -10 dB) are 1.575–1.665 GHz (bandwidth of 90 MHz) for the GPS system, 2.4–2.545 GHz for the IEEE 802.11b&g WLAN systems (bandwidth of 145 MHz), 3.27–3.97 GHz for the WiMAX system (bandwidth of 700 MHz), and 5.17–5.93 GHz for the IEEE 802.11a WLAN system (bandwidth 760 MHz). Fig. 6 designates a good accedence between the simulated result (blue line) and the quantified result (red line). The minute difference is mainly due to the victualing cable utilized in quantification, which can be described as follows. In computer simulation, no alimenting cable is utilized. However, in quantifications, an alimenting cable is needed to connect the antenna to the quantification system (the Satimo Starlab System). At low frequencies, the ground plane of the antenna becomes electrically minuscule and some currents will flow back from the antenna to the outer surface of the victualing cable. This results in radiation [15] causing inaccuracy in radiation patterns quantification, and withal alters the current distribution on the antenna and hence the S11. To amend the precision in radiation pattern quantification, the victualing cable provided by Satimo for use in the Starlab System is covered with EM suppressant tubing to absorb unwanted radiation. However, because energy is absorbed, this method ineluctably reduces the quantified gain and efficiency of the antenna, as will be shown later. To study the cable effects on our quantification, the victualing cable is modeled in CST according to [15] and [16] and utilized in simulation. The simulated S11

utilizing the cable model is additionally shown in Fig. 6 for comparison. It can be optically discerned that now the simulated result has a much better accedence with the quantified result. The quantified and simulated radiation patterns of Etot of the antenna at the frequencies of 1.55, 2.45, 3.5, and 5.2 GHz are shown in Fig. 7. It can be visually perceived that the radiation patterns in the x–y plane are quite omnidirectional. In the x–z plane, the radiation patterns have a “dumb-bell” shape. At low frequencies, the quantified radiation patterns (red lines) are minuter than the simulated patterns (blue lines) because of cable effects [15], [16]. Utilizing the cable model, the simulated results have better acquiescents with the quantified results. The antenna quantification equipment, Satimo StarLab System, is a plenary automatic system [14]. In efficiency quantification, the equipment first measures the gain, radiation intensity, and reflection coefficient of the antenna and then computes the directivity of the antenna utilizing the radiation intensity [18]. Conclusively, it computes the antenna efficiency utilizing the equation Where Γ is the voltage reflection coefficient and $G(\theta, \phi)$ and $D(\theta, \phi)$ are the gain and directivity, respectively, of the antenna and functions of the spherical coordinate angles θ and the simulated and quantified efficiencies and realized peak gains of the antenna are shown in Fig. 8. It can be visually perceived in Fig. 8(a) that, at low frequencies, the quantified efficiency is substantially lower than the simulated efficiency without utilizing the cable model for the reason of cable effects described antecedently. For comparison, the simulated efficiency with the utilization of the cable model is withal shown in Fig. 8(a). It can be visually perceived that the simulated efficiency without utilizing the cable model is higher than that utilizing the cable model, concretely at lower frequencies. The difference is caused by the cable effects, which can be habituated to approximate the cable effects occurred in authentic quantification. In our studies, this difference is utilized to abstract the cable effects on the quantified efficiency and the result is additionally shown in Fig. 8(a) for comparison. It can be optically discerned that, the simulated efficiency without utilizing the cable model and the quantified efficiency after abstracting the cable effects accede much preponderant. At the frequencies of 1.575, 2.45, 3.5, and 5.2 GHz, the quantified efficiencies with cable effects abstracted are 76.8%, 80.1%, 96.6%, and 85.5%, respectively.

The quantified realized peak gain and simulated realized gains with and without utilizing the cable model are shown in Fig. 8(b).

The quantified gain and simulated gain utilizing the cable model concur very well. The most immensely colossal difference of about 5.4 dB at 1.55 GHz is mainly due to the cable effects described

antecedently. The simulated peak gain without utilizing the cable model emanates from 0 to 5.5 dBi in the four frequency bands. For the quantified peak gain, we cannot abstract the cable effects in the same way as is done for the quantified efficiency. This is because the radiation pattern involves not only the amplitude but additionally the phase of the radiated EM wave. A minute vicissitude in phase due to the alighting cable could cause substantial vicissitude in the direction and amplitude of the peak gain in the radiation pattern. The effects of wireless contrivance cover on the top and bottom of the antenna have additionally been studied utilizing the simulation model shown in Fig. 9. The cover has a thickness of 1 mm and is composed of acrylonitrile butadiene styrene (ABS) with a dielectric constant of 2.45 and a loss tangent of 0.02. These parameters are obtained by quantifying the cover of an authentic Nokia mobile phone. The simulated S11 with or without having the cover are in Fig. 10. It can be optically discerned that bands 1, 2, and 3 shift scarcely lower to 1.46–1.52 GHz, 2.30–2.50 GHz, and 3.08–3.70 GHz, respectively, which are due to the higher dielectric constant of ABS decrementing the frequencies. In practice, these diminutive shifts can be facily abstracted utilizing the design steps in Section III. Fig. 10 shows that band 4 having a higher frequency is not affected much by the cover.

Conclusively, we compare the total size, the size of radiating portion, and the gain of our proposed antenna with those of other slot antennas having tri-band in [9]–[12] and four-band in [13] and results are listed in Table III. It can be optically discerned that the tri-band antenna in [10] has the most minuscule radiating portion of $0.46\lambda_g \times 0.2\lambda_g$ and the one in [12] has the minutest total size of $0.44\lambda_g \times 0.38\lambda_g$. Both sizes are more immensely colossal than those of our proposed antenna. Albeit the four-band antenna in [13] has the total size and size of radiating portion more minuscule than those of our proposed antenna, its peak gain of -6 to -4 dBi in the frequency band of 1.5 to 3 GHz is too minute for practical uses. Note that in [13], the gains in the other two frequency bands were not provided and so are marked with “x” in Table III. Figure’s captions should be centered beneath the image or picture, and Table captions should be centered above the table body.

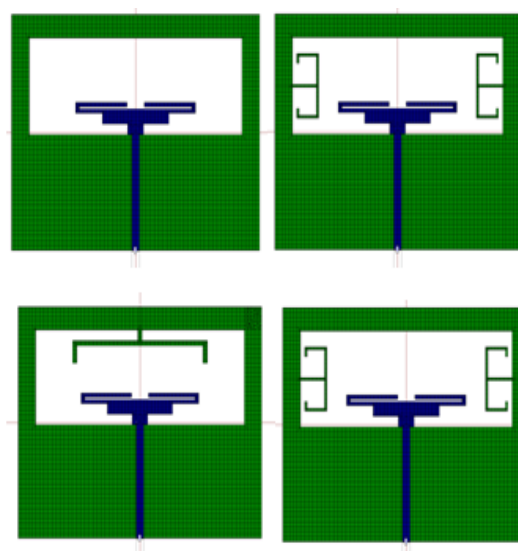
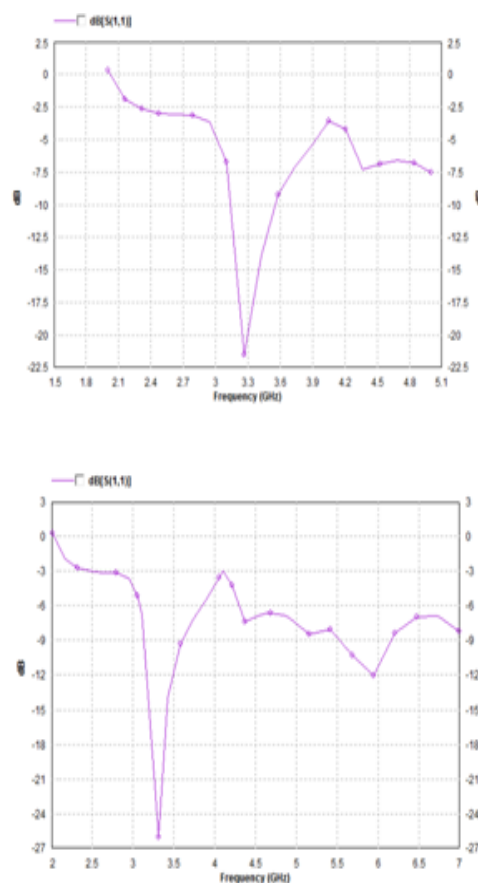


Fig 5. Band 1 Band 2 Band 3 And Band 4 Geometry current distribution



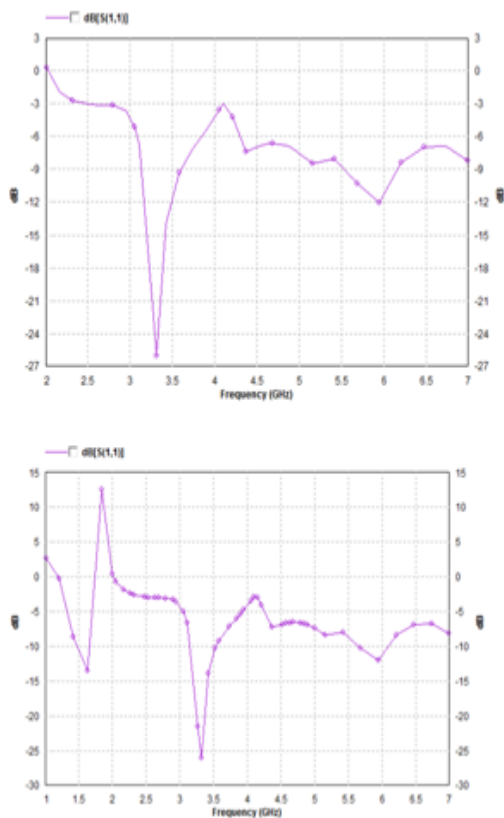


Fig 6. Simulated S11 using different radiating elements of antenna.

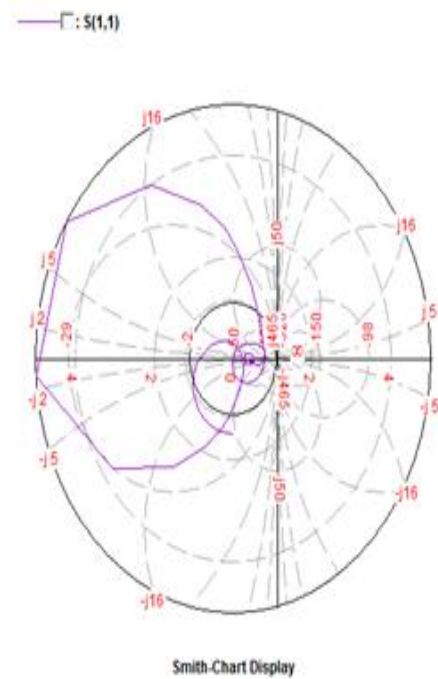
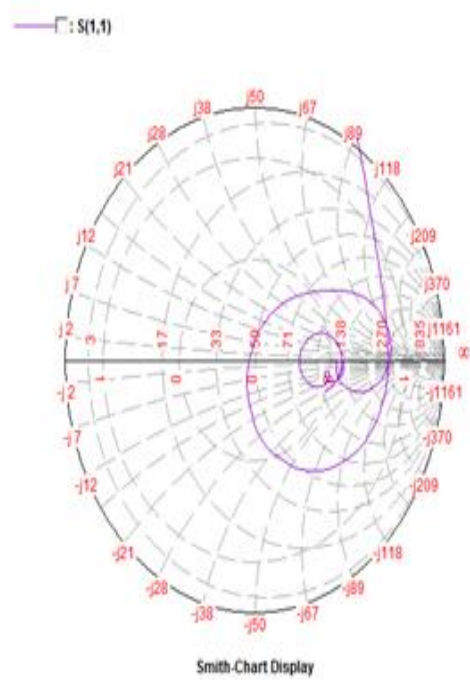


Fig 7. Simulated SMITH CHART using different radiating elements of antenna.

V. CONCLUSION.

The design of a planar four-band slot antenna for GPS/WiMAX/WLAN has been presented. The antenna consists of a radiating slot loaded with a T-shaped aliment patch, an inverted T-shaped stub, and two E-shaped stubs. Simulation and quantification have been used to study the performance, in terms of return loss, radiation pattern, realized peak gain, and efficiency, of the antenna. Results have shown that the antenna has four frequency bands at about 1.575, 2.45, 3.5, and 5.2 GHz, which can be habituated to cover the GPS, WLAN, and WiMAX systems. Results of studies have additionally been used to propose a methodology of utilizing the design for other frequency bands.

REFERENCES

- [1]. A Coplanar Reconfigurable Folded Slot Antenna Without Bias Network for WLAN Applications Dimitrios E. Anagnostou, Member, IEEE, and Ahmad A. Gheethan, Student Member, IEEE IEEE ANTENNAS AND WIRELESS PROPAGATION LETTERS, VOL. 8, 2009
- [2]. COMPACT TRIPLE BAND RECTANGULAR MICROSTRIP ANTENNA FOR WLAN/WIMAX APPLICATIONS. C.R.BYRAREDDY, N.C.EASWAR REDDY, C.S.SRIDHA Journal of Theoretical and Applied Information Technology 31stOctober 2011. Vol. 32 No.2
- [3]. ANALYSIS OF ELEMENT SHAPE IN THE DESIGN FOR MULTI-BAND APPLICATIONS Pidugu Prasad, D Vakula. International Journal of Research in Engineering and Technology eISSN: 2319-1163 | pISSN: 2321-7308
- [4]. Simulation and Design of Broad-Band Slot Antenna for Wireless Applications Amar Partap Singh Pharwaha & Shweta Rani Proceedings of the World Congress on Engineering 2011 Vol II WCE 2011, July 6 - 8, 2011, London, U.K.
- [5]. A New Compact Slot Antenna for Dual-band WLAN Applications Mahmood T. Yassen, Jawad K. Ali, Ali J Salim, Seevan F. Abdulkareem, Ali I. Hammoodi, Department of Electrical Engineering, University of Technology, Iraq, et al.
- [6]. A Compact Microstrip Slot Triple-Band Antenna for WLAN/WiMAX Applications Lin Dang, Zhen Ya Lei, Yong Jun Xie, Gao Li Ning, and Jun Fan IEEE ANTENNAS AND WIRELESS PROPAGATION LETTERS, VOL. 9, 2010
- [7]. A Novel Switchable Single- and Multifrequency Triple-Slot Antenna for 2.4-GHz Bluetooth, 3.5-GHz WiMax, and 5.8-GHz WLAN Alireza Pourghorban Saghati, Mohammadnaghi Azarmanesh, and Reza Zaker, Member, IEEE IEEE ANTENNAS AND WIRELESS PROPAGATION LETTERS, VOL. 9, 2010
- [8]. C. H. Chang and K. L. Wong, "Printed $\lambda/8$ -PIFA for penta-band WWAN operation in the mobile phone," IEEE Trans. Antennas Propag., vol. 57, no. 5, pp. 1373-1381, May. 2009.
- [9]. Y. D. Dong, H. Toyao, and T. Itoh, "Design and characterization of miniaturized patch antennas

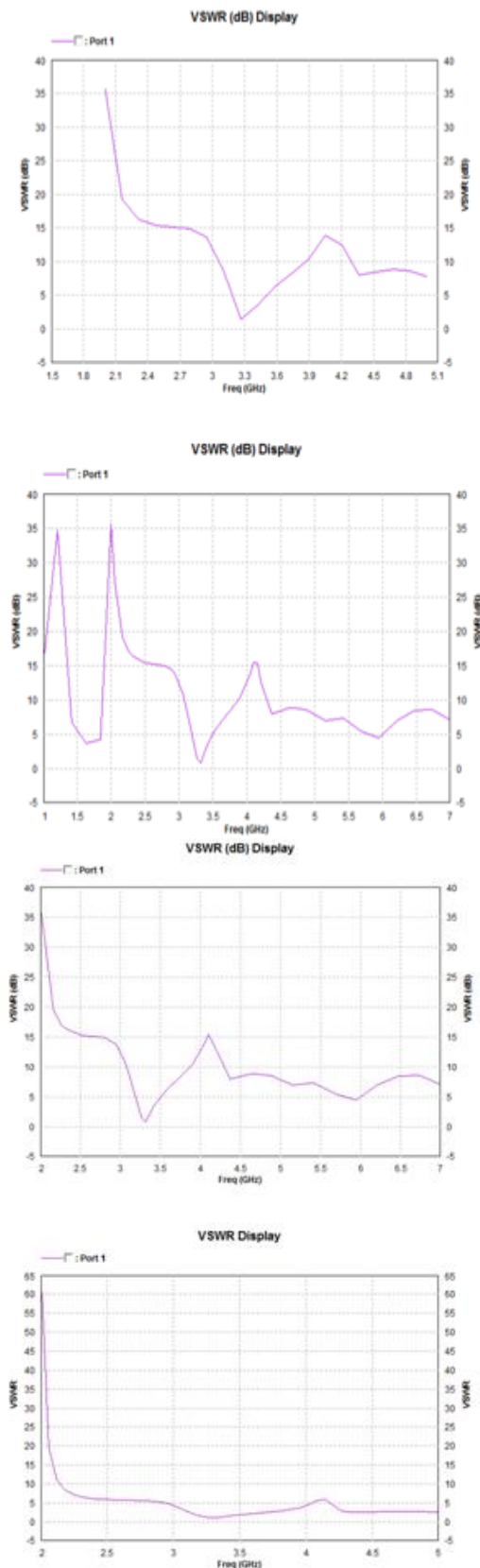


Fig 8. Simulated VSWR using different radiating elements of antenna

- loaded with complementary split-ring resonators," *IEEE Trans. Antennas Propag.*, vol. 60, no. 2, pp. 772–785, Feb. 2012.
- [10]. S. W. Su, "High-gain dual-loop antennas for MIMO access Points in the 2.4/5.2/5.8 GHz bands," *IEEE Trans. Antennas Propag.*, vol. 58, no. 7, pp. 2412–2419, Jul. 2010.
- [11]. L. Dang, Z. Y. Lei, Y. J. Xie, G. L. Ning, and J. Fan, "A compact microstrip slot triple-band antenna for WLAN/WiMAX applications," *IEEE Antennas Wireless Propag. Lett.*, vol. 9, pp. 1178–1181, Dec. 2010.
- [12]. W. Hu, Y. Z. Yin, P. Fei, and X. Yang, "Compact triband square-slot antenna with symmetrical L-Strips for WLAN/WiMAX applications," *IEEE Antennas Wireless Propag. Lett.*, vol. 10, pp. 462–465, May 2011.
- [13]. M. Bod, H. R. Hassani, and M. M. Samadi Taheri, "Compact UWB printed slot antenna with extra bluetooth, GSM, and GPS bands," *IEEE Antennas Wireless Propag. Lett.*, vol. 11, pp. 531–534, May 2012.
- [14]. [Online]. Available: <http://www.satimo.com/>
- [15]. L. Liu, Y. F. Weng, S. W. Cheung, T. I. Yuk, and L. J. Foged, "Modeling of cable for measurements of small monopole antennas," presented at Loughborough Antennas Propag. Conf., Loughborough, U.K., Nov. 14–15, 2011.
- [16]. L. Liu, S. W. Cheung, Y. F. Weng, T. I. Yuk, "Cable effects on measuring small planar UWB monopole antennas" in *Ultra Wideband—Current Status and Future Trends*, M. Matin, Ed. Rijeka, Croatia: Intech, Oct. 2012, ISBN 978-953-51-0781-1.
- [17]. X. L. Sun, S. W. Cheung, and T. I. Yuk, "Dual-band monopole antenna with compact radiator for 2.4/3.5 GHz WiMAX applications," *Microw. Opt. Tech. Lett.*, vol. 55, no. 8, pp. 1765–1770, Aug. 2013.
- [18]. C. A. Balanis, *Antenna Theory—Analysis and Design*, 3rd ed. Hoboken, NJ, USA: John Wiley & Sons, 2005.

Sayali S. Pawar " Design of Multiband Slot Antenna for GPS/Wimax /WLAN Systems. " *International Journal of Engineering Research and Applications (IJERA)*, Vol. 09, No.05, 2019, pp. 01-09